Experimental and Calculated Spectra of π-Stacked Mild Charge-Transfer Complexes: Jet-cooled Perylene·(Tetrachloroethene)$_n$, $n = 1, 2$

Franziska A. Balmer, Philipp Ottiger, and Samuel Leutwyler*

Department of Chemistry and Biochemistry, University of Bern, Freiestrasse 3, CH-3012 Bern, Switzerland

E-mail: leutwyler@dcb.unibe.ch

Abstract

The $S_0 \leftrightarrow S_1$ spectra of the mild charge-transfer (CT) complexes perylene·tetrachloroethene (P·4ClE) and perylene·(tetrachloroethene)$_2$, P·(4ClE)$_2$, are investigated by two-color resonant two-photon ionization (2C-R2PI) and dispersed fluorescence spectroscopy in supersonic jets. The $S_0 \rightarrow S_1$ vibrationless transitions of P·4ClE and P·(4ClE)$_2$ are shifted by $\delta\nu = -451$ and -858 cm^{-1} relative to perylene, translating to excited state dissociation energy increases of 5.4 and 10.3 kJ/mol, respectively. The redshift is $\sim$ 30% larger than that of perylene·*trans*-1,2-dichloroethene, so the increase in chlorination increases the excited-state stabilization and charge-transfer character of the interaction, but the electronic excitation remains largely confined to the perylene moiety. The 2C-R2PI and fluorescence spectra of P·4ClE exhibit strong progressions in the perylene intramolecular twist ($1a_u$) vibration (42 cm^{-1} in S_0 and 55 cm^{-1} in S_1), signaling that perylene deforms along its twist coordinate upon electronic excitation. The intermolecular stretching (T_z) and internal-rotation (R_c) vibrations are weak, so

*To whom correspondence should be addressed

the P·4ClE intermolecular potential energy surface changes little during the $S_0 \leftrightarrow S_1$ transition. The minimum-energy structures and inter- and intramolecular vibrational frequencies of P·4ClE and P·$(4ClE)_2$ are calculated with the dispersion-corrected density functional theory (DFT) methods B97-D3, ωB97X-D, M06 and M06-2X and the spin-consistent-scaled (SCS) variant of the approximate second-order coupled-cluster method, SCS-CC2. All methods predict the global minima to be π-stacked centered co-planar structures with the long axis of tetrachloroethene rotated by $\tau \sim 60^\circ$ relative to the perylene long axis. The calculated binding energies are in the range $-D_0 = 28 - 35$ kJ/mol. A second minimum is predicted with $\tau \sim 25^\circ$, with ~ 1 kJ/mol smaller binding energy. Although both monomers are achiral, both the P·4ClE and P·$(4ClE)_2$ complexes are chiral. The best agreement for adiabatic excitation energies and vibrational frequencies is observed for the ωB97X-D and M06-2X DFT methods.

Keywords: perylene, charge transfer, π-stacking, tetrachloroethene, chirality, supersonic jet, gas phase, laser spectroscopy

1 Introduction

The concept of intermolecular charge-transfer (CT) electronic transitions was introduced by Mulliken in 1952 and has remained a widely studied subject.[1–5] Perylene based charge-transfer complexes are well suited for investigating CT excitations, since it is a planar aromatic with a large adsorption area for planar acceptor molecules and a low adiabatic ionization potential AIP$= 6.96$ eV,[6] which makes it a good π-electron donor.[6,7] Finally, perylene has a well-characterized vibronic spectrum.[7–15] These properties allow to investigate a range of different acceptor molecules on the charge-transfer transitions. We previously reported the vibronic spectra of the mild CT complex perylene·*trans*-1,2-dichloroethene.[7]

Bare ethene has a negative vertical electron affinity ($EA = -1.73$ eV) and does not stabilize an excess electron.[16] Substituting its hydrogen atoms with one to four Cl atoms renders the EA *less* negative, as shown in Table 1, because the chlorine atoms increasingly remove electron density from the C=C bonds and stabilize the lowest unoccupied molecular orbital (LUMO). The exper-

imental electron affinity of *trans*-1,2-dichloroethene (2ClE) is $EA = -0.80$ eV and falls about halfway between ethene ($EA = -1.73$ eV) and tetrachloroethene ($EA = -0.30$ eV).[16]

The $S_0 \rightarrow S_1$ spectrum of perylene·1,2-dichloroethene (P·2ClE) is redshifted by $\delta\nu = -307$ cm^{-1} relative to that of bare perylene, corresponding to excited-state stabilization of 3.67 kJ/mol, and indicating a mild charge-transfer from the highest occupied molecular orbital (HOMO) of perylene to the LUMO of 1,2-dichloroethene.[7] The S_1 state geometry of P·2ClE is strongly displaced along the internal-rotation coordinate that rotates 1,2-dichloroethene around its C_2 axis relative to the perylene surface normal.[7]

In this work, we explore the effect of increase in chlorination on the charge-transfer excitation in perylene·tetrachloroethene and in the perylene·(tetrachloroethene)$_2$ sandwich cluster, in which the donor perylene is complexed from both sides. Topp and coworkers have shown that perylene complexes with one and with two solvent (S) molecules that are van-der-Waals dispersively bonded to opposite sides (the so-called trans 1:2 complexes) exhibit spectral redshifts that are closely additive. Thus, the ratio of the redshift of the 1:2 relative to the 1:1 perylene·S complexes are between 1.85 to 1.95 for tetramethylsilane,[12] butadiene,[12] 1-chlorobutane,[13] benzene[13] and 1-chloropentane.[13] In contrast a cis-isomer was observed for perylene·(ethene)$_2$ with both ethene units adsorbing on the same side of perylene. Tetrachloroethene is a much better electron acceptor than ethene, giving rise to the question whether two tetrachloroethene preferentially interact with perylene as the trans (sandwich) or as the cis-isomer.

2 Methods

2.1 Experimental Methods

Perylene·tetrachloroethene complexes were synthesized and cooled in a 20 Hz supersonic jet expansion, using neon as a carrier gas with a backing pressure of 1.2 bar. Perylene (Fluka, $> 99\%$ purity) was heated to 180°C in the sample holder of the pulsed nozzle. Tetrachloroethene (Fluka, purum) was cooled in a bubbler to 0°C (5 mbar partial pressure), through which the Ne carrier

gas was passed. Mass-selective $S_0(^1A) \rightarrow S_1(^1B)$ vibronic spectra were measured in the region of $23100 - 24300$ cm^{-1} by the two-color resonant two-photon ionization (2C-R2PI) technique as described elsewhere.[7]

Excitation was performed with the of a Nd:YAG pumped Lambda Physik FL3000 laser using Stilbene 420 in EtOH; the output pulse energy was reduced to ($\sim 20\mu$J/pulse) in order to avoid optical saturation of the very strong perylene $S_0 \rightarrow S_1$ transition. In order to measure the weak signals of the perylene·(tetrachloroethene)$_2$ cluster, the excitation laser power was again raised by a factor 10. The bandwidth was 0.3 cm^{-1} as measured with a HighFinesse Ångstrom WS6 high precision wavemeter. The excited molecules were ionized by the 266 nm (1 mJ/pulse) of the same Nd:YAG pump laser. The spectra were recorded with a step size of 0.4 cm^{-1} and averaged over 20 laser shots.

Dispersed fluorescence (DF) spectra of perylene·tetrachloroethene were obtained by probing the complexes with laser excitation at the 0_0^0 band (23609 cm^{-1}), see below.

2.2 Computational Methods

Dispersive interactions play an important role for the correct description of non-covalently bound complexes, and this has been included into density-functional theory (DFT) methods by adding empirical atom–atom dispersion corrections.[17–19] As previously, we used the Grimme dispersion-corrected density functional method B97-D3 with the def2-TZVPP basis set for the electronic ground state (no excited-state variant of B97-D3 has so far been developed).[19] The Minnesota functionals M06 and M06-2X[18] which include different amounts of exchange correlation, and the Chai and Gordon dispersion- and long-range-corrected ωB97X-D functional were also employed,[20] using the 6-31++G(d,p) basis set. The corresponding time-dependent (TD) DFT methods were employed for the S_1 state calculations.

To benchmark the (time-dependent) DFT methods we employed the correlated spin-component-scaled SCS-CC2 method. The SCS variant was used, since conventional MP2 and CC2 methods lead to grossly overestimated binding energies for π-stacked complexes. In contrast, for the stacked

benzene dimer[21] as well as for a series of stacked 2-pyridone-fluorobenzene complexes the SCS-MP2 binding energies were found to be in good agreement with the CCSD(T) values.[22,23] Due to the high computational cost, the TZVP basis set was initially used for the S_0 and S_1 state structure optimizations. The S_0 state binding energy at the TZVP-optimized structure was then recalculated with the def2-TZVPP and QZVP basis sets, and the basis set superposition error (BSSE) determined as a function of basis set size. The S_0 state harmonic vibrational analysis was performed at the SCS-CC2/TZVP level. Structure optimizations for the P·(4ClE)$_2$ sandwich complex were performed with B97-D3, ωB97X-D and M06-2X, and for the S_0 ground state only.

For each optimized structure the S_0 and S_1 state binding energies D_e and zero-point energy (ZPE) corrected binding energies D_0 were calculated with and without the Boys-Bernardi counterpoise (CP) correction.[24] The B97-D3 and SCS-CC2 calculations were carried out using the Turbomole 6.3 program package.[25] All other calculations were performed using Gaussian09.[26]

The performance of the different methods was evaluated by comparing the calculated adiabatic excitation energies (E_{ex}) and vibrational normal-mode frequencies of the P·4ClE complex to the experimental values. To quantify the performance of the different methods with respect to the vibrational frequencies, the root-mean-square deviation (RMSD) of the calculated to the experimental frequencies was determined.

3 Computational Results

3.1 Ground State Structures and Binding Energies

The S_0-state structure optimizations of P·4ClE resulted in two structures shown in Figure 1. All computational methods except for M06 agree that in the global minimum structure **M1** the tetrachloroethene long axis is rotated by $\omega \sim 60^\circ$ relative to the perylene long (x) axis. In the local minimum that we denote **M2**, it is rotated by $\omega \sim 25^\circ$. The M06 calculation predicts a single minimum structure at a rotation angle of 45.8°. The rotation angles ω are listed in Table 2.

In both the **M1** and **M2** structures, the perylene and tetrachloroethene moieties are nearly

coplanar with their centers of mass aligned along the respective surface normals. The π-stacking interaction twists the perylene moiety out-of-plane. This twist deformation is well described by the lowest-frequency intramolecular $1a_u$ vibration of perylene; the calculated twist angles are $\tau = 3 - 11^\circ$. Both structures are C_2-symmetric, consequently, both **M1** and **M2** have two symmetry-equivalent and degenerate chiral forms. Given that the **M1** and **M2** structures differ mainly with respect to ω, it is probable that the potential of the R_c mode (which corresponds to a change in ω) is very flat. Details of the vibrational modes are discussed below.

The calculated interplanar distance between the center-of-mass of perylene and tetrachloroethene are between $R_{COM} = 3.34$ and 3.48 Å for the **M1** structure, while the interplanar distances in the **M2** structures are very slightly $0.003 - 0.016$ Å longer. Some characteristic structure parameters predicted by the different methods are listed in Table 2.

The binding energies D_e at the **M1** and **M2** geometries were calculated with and without counterpoise (CP) corrections and are listed in Table 3. The largest binding energy ($-D_e = 37.5$ kJ/mol) is predicted by the B97-D3 method. Counterpoise corrections are not recommended for this method,,[27] the uncorrected binding energy indeed agrees well with the CP-corrected binding energies of the other methods. The other three dispersion-corrected density functional methods (M06, M06-2X and ωB97X-D) yielded CP-corrected binding energies $-D_e^{CPC}$ between 31 and 36 kJ/mol for the **M1** structure. The uncorrected binding energies differ more strongly, with BSSEs ranging from 7 to 9 kJ/mol for the DFT methods. The SCS-CC2 binding energy with the TZVP basis set is only 111.6 kJ/mol, due to overcorrection by the large BSSE (56.4 kJ/mol). As Table 3 shows, the BSSE decreases strongly when increasing the basis set to def2-TZVPP and QZVP.

Since the sizable BSSE with the TZVP basis set is expected to affect the structure, we recalculated the intermolecular center-of-mass distance R_{COM} by displacing the TZVP-optimized perylene and tetrachloroethene moieties in steps of 0.1 Å along the z-coordinate of the complex and calculated the binding energy and BSSE pointwise with the def2-TZVPP basis set. The minimum of the resulting potential energy curve is at $R_{COM,min} = 3.35$ Å rather than 3.23 Å as predicted by the TZVP basis set. The same procedure was carried out for the local minimum **M2** and for the

first excited state. Table 3 shows that all methods predict a smaller binding energy for the local minimum **M2** compared to the rotamer **M1**, but the differences in D_0^{CPC} are small: 0.7 kJ/mol with B97-D3, 1.86 kJ/mol with ωB97X-D, , 0.82 kJ/mol with M06-2X and 0.25 kJ/mol with SCS-CC2.

3.2 Excited State Structure and Binding Energies

The S_1 state optimizations were started from the S_0 state **M1** and **M2** geometries and resulted in C-C bond length changes within the perylene moiety that are very similar to those calculated for bare perylene.[7] All methods agree that the bond lengths of the core bonds of perylene shorten by $0.02 - 0.04$ Å. The τ twist angle decreases upon $S_0 \rightarrow S_1$ excitation. This is due to the change in intermolecular distance: The perylene and tetrachloroethene units move closer together upon excitation, while the C_2-symmetry is maintained. The intermolecular distance between the centers of mass (R_{COM}) is predicted to decrease by $\Delta R_{COM} = 0.03 - 0.06$ Å upon excitation. The approach of the tetrachloroethene unit tends to flatten the perylene surface. The bond lengths within the tetrachloroethene unit remain virtually unchanged and the dihedral angles change by 0.2° at most. This indicates that the electronic excitation is largely localized within the perylene subunit, similar to perylene·1,2-dichloroethene, indicating a rather weak CT interaction.

The counterpoise-corrected excited state binding energies D_e^{CPC} and the ZPE-corrected D_0^{CPC} binding energies are listed in Table 3. The binding energies of the **M1** structure increase upon $S_0 \rightarrow S_1$ excitation. This increase in D_0^{CPC} corresponds to a spectral redshift of the P·4ClE $S_0 \rightarrow S_1$ transition, relative to that of perylene. The predicted shifts vary quite widely between methods, ΔD_e^{CPC} being -221 cm^{-1}(2.64 kJ/mol increase) with M06, -204 cm^{-1} (2.44 kJ/mol) with M06-2X, -176 cm^{-1} (2.11 kJ/mol) with ωB97X-D and -293 cm^{-1} (3.19 kJ/mol) with SCS-CC2. The latter prediction is closest to the experimentally observed redshift of $-\delta\nu = -451$ cm^{-1}. The SCS-CC2 $D_0^{CPC}(S_1)$ is corrected with the ωB97X-D S_1 state ZPE, because SCS-CC2 excited-state vibrational calculations vastly exceed our computational capacities. The S_0 state ZPE of ωB97X-D is very close to that of the S_0 state SCS-CC2 calculation. The agreement of the calculated shifts with experiment is far from impressive, indicating need for improvement.

3.3 Normal Mode Analysis

The harmonic vibrational calculations were performed at the optimized **M1** and **M2** geometries using the same methods and basis sets. The vibrational modes of perylene are discussed elsewhere.[7,15] Since the totally-symmetric (a_g in D_{2h}) vibrations of perylene contribute strongly to the vibronic spectra of the complex, they are referred to by their irreducible representation in bare perylene. Excitations in perylene out-of-plane vibrations such as the $1a_u$, $1b_{1u}$ and $2a_u$ modes will be color-coded for ease of comparison. Six intermolecular normal modes are generated upon complexation, which are grouped into three hindered rotational modes (R_a, R_b, R_c) and three hindered translational modes (T_x, T_y, T_z), following the classification of Topp and co-workers.[28] The translational modes comprise two bends (T_x, T_y) and an intermolecular stretch (T_z), the rotational normal modes are grouped into two rocking motions (R_a, R_b) and a rotation about the perylene surface normal (R_c).[28] These intermolecular normal-mode eigenvectors are shown in Figure 2. The calculated and experimental frequencies are shown in Tables 4 and 5 and will be discussed in conjunction with the spectra.

The structural changes upon $S_0 \rightarrow S_1$ excitation, which are given in Table 2, indicate which intra- and intermolecular vibrations should appear in the vibronic spectrum: (1) Since the τ twist angle around the perylene x-axis changes, excitations of the $1a_u$ twist mode are expected. (2) The decrease of the stacking distance between perylene and tetrachloroethene should give rise to the T_z interplanar stretching mode. (3) The change of the rotation angle of tetrachloroethene relative to perylene is between $\omega = 1^\circ$ and 6°, suggesting that the R_c mode should appear.

4 Experimental Results

4.1 Perylene·tetrachloroethene R2PI spectrum

The complexation with tetrachloroethene renders the vibronic spectrum much more complex than that of perylene, since the local symmetry is reduced from D_{2h} to C_2, with many more totally-

symmetric vibrations in the complex than in perylene. The R2PI spectra of perylene·tetrachloroethene and of perylene·(tetrachloroethene)$_2$ are shown in Figure 3. The R2PI spectra exhibit a rich vibronic band structure on top of broad background structure. A part of this background is due to optical saturation and can be reduced by decreasing the intensity of the excitation laser, as in Figures 4 and 5.

The P·4ClE 0_0^0 band is observed at 23609 cm^{-1} and is redshifted by $\delta\nu = -451$ cm^{-1} relative to the perylene 0_0^0 at 24060 cm^{-1}. For ease of comparison, the 2C-R2PI spectrum is separated into sections of 350 cm^{-1} length in Figures 4 and 5, and plotted above the respective sections of the bare perylene spectrum with the respective electronic origins set to zero. The vibronic band contours have a full width at half maximum (FWHM) of $\sim$ 1.3 cm^{-1}, reflecting a rotational temperature of $T_{rot} = 2 - 3$ K. Note the appearance of weak hot bands and sequence bands below and above the electronic origin band. Together with the background features, discussed in more detail below, they imply that the vibrational temperature is higher, $T_{vib} \sim 15$ K.

The spectrum is dominated by a vibrational progression with a 55 cm^{-1} fundamental that is assigned to the perylene $1a_u'$ excited-state twist mode. This vibration is expected to appear due to changes of the intramolecular τ twist angle of perylene. Due to the $D_{2h} \rightarrow C_2$ symmetry descent, the non-totally symmetric $1a_u$ vibration becomes totally-symmetric (a) in the complex, and the fundamental band now appears strongly in the R2PI spectrum, see Figures 4 and 5. The calculations predict $1a_u'$ frequencies of 66 cm^{-1} (ωB97X-D), 70 cm^{-1} (M06-2X) and 71 cm^{-1} (M06). The low-frequency $1b_{1u}'$ out-of-plane vibration of perylene also becomes totally-symmetric (a) in the complex giving rise to a weak fundamental at 95 cm^{-1}.

The lowest-frequency bands in Figures 4(a) and 5(a) are weak and exhibit a frequency of 11 cm^{-1}. Based on the low frequency, we assign these to the intermolecular R_c' vibration. The calculated S_1 harmonic frequencies of 17 cm^{-1} (ωB97X-D) and 29 cm^{-1} (M06-2X) are overestimated since the intermolecular potential energy surface is extremely flat and anharmonic along the R_c coordinate, as will be discussed below. We assign the progression with a 60 cm^{-1} fundamental frequency to the intermolecular stretch T_z'. Several combinations with members of the $1a_g'$ progres-

sion can identified, see Figure 4(a). The frequency is in acceptable agreement with the calculated harmonic frequencies of 73 cm^{-1}(ωB97X-D) and 78 cm^{-1} (M06-2X). Further combination bands of the $1a'_u$ perylene twist with the intermolecular T'_z vibration also appear strongly in the spectrum.

In the $300 - 650$ cm^{-1} section of the spectrum shown in Figure 5, the vibronic structure is repeated in combination with the intense $1a'_g$ perylene intramolecular fundamental mode at 351 cm^{-1}, similar as has been observed for perylene·1,2-dichloroethene.[7] The $1a_g$ vibration is the lowest-frequency totally-symmetric vibration of perylene, corresponding to a x-stretching motion. Also the second and third totally symmetric perylene modes are well discernible. The perylene out-of-plane $2a'_u$ mode (marked in orange) is clearly visible in the high energy part of the spectrum (Figure 5), where it forms a Fermi resonance with the $3a'_g$ band. By contrast, in the low energy part of the spectrum it is hardly discernible. The full assignment is listed in Table 4.

At this point we need to discuss the broad background signal observed beneath - but not coincident with - the sharp vibronic bands in Figure 4, since it has important implications for the interpretation of the intermolecular vibronic excitations. One hypothesis for the existence of the background is that it arises from P·(4ClE)$_2$ or larger clusters decaying into the P·(4ClE)$^+$ mass channel. Figure 3 compares the two-color R2PI signals recorded in the mass channels of (a) P·4ClE and (b) P·(4ClE)$_2$. The spectrum of P·(4ClE)$_2$ is redshifted by 405 cm^{-1} relative to that of P·4ClE. Weak fragment ion signal from the P·(4ClE)$_2^+$ $\rightarrow$P·4ClE$^+$ can indeed be observed in the wavenumber region $23200-23600$ cm^{-1}, but this contribution is $< 5\%$ of the P·4ClE. Subtracting the scaled P·(4ClE)$_2$ spectrum from the P·4ClE spectrum showed that this contribution is hardly even visible on the scale of Figure 3(a).

A second hypothesis is that this part of the spectrum arises from complexes that are fluxional and undergo large-amplitude rotational/translational motions because of low rotational/translational barriers in the S_0 -state intermolecular potential energy surface (IPES). Given the existence of the **M1** and **M2** minima that differ mainly by a $\omega \sim 35^\circ$ relative rotation, which is a displacement that is well described by the intermolecular R_c normal coordinate (see Figure 1 and Table 6) we will focus on this intermolecular coordinate. Depending on the computational method and on the basis

set as well as the chosen interplanar distance R_{COM}, the calculated **M1** and **M2** minimum energies differ between 0.25 and 1.31 kJ/mol, the minimum angles ω_{min}(**M1**) and ω_{min}(**M2**) differ by up to 9°. The existence of two chiral enantiomers for both **M1** and **M2** implies that there are two inequivalent pairs of minima (i.e., **M1/M1'** and **M2 /M2'**) along the R_c intermolecular rotational coordinate. Figure 6 shows a generic S_0 IPES intended to capture the qualitative features along the R_c coordinate and will be discussed in more detail below.

A vibronic spectrum was simulated with the PGOPHER 7.0 program[29] based on the ωB97X-D S_0 and S_1 state calculations for the **M1** structure, and is shown in Figure 7. The Franck-Condon factors (FCF) of the $1a'_u$ progression are predicted in good agreement with the assignment above, as are the T'_z excitations. In contrast, the FCFs of the R'_c mode are strongly overestimated, which indicates that the change in ω upon $S_0 \rightarrow S_1$ excitation is overestimated by the calculation. The appearance of in-plane translational T'_x vibrational bands is also overestimated relative to the experiment, probably due to the fact that the T_x vibration also has a very shallow potential.

The PGOPHER analysis allowed identification of anharmonicity of the $1a'_u$ and T'_z vibrations, as well as the assignment of hot bands and sequence bands $(R_c)^1_0$, $(R_c)^2_1$, $(R_c)^1_1$ and $(T_z)^1_1$, as listed in Table 4. These hot and sequence bands are also found in combination with a multitude of bands, contributing to the elevation of the background around the origin and the $1a'_u$- and T'_z-progressions.

A second PGOPHER vibronic band simulation based on the local minimum **M2** is shown in Figure 7(b). The agreement with the experimental R2PI spectrum is poor, the calculated FCFs are much worse compared to the **M1** simulation. Several fundamental transitions are weaker than the respective overtones, which is not the case in the experimental spectrum. Additionally, the hot bands are not reproduced as well as in **M1**. Overall, the PGOPHER simulation of **M1** is much closer to the experiment than that for **M2** simulation, agreeing with the prediction of global and local minima.

4.2 Perylene·tetrachloroethene fluorescence spectrum

The dispersed fluorescence (DF) spectrum of P·4ClE is shown in the same manner as the 2C-R2PI spectra; a section of 350 cm^{-1} alongside the corresponding bare perylene DF spectrum for the origin region (Figure 8). The spectrum of the high energy region can be found in the Supplemental Material. By means of the 2C-R2PI spectrum and PGOPHER[29] simulations, a tentative assignment was made. The spectrum exhibits a two-membered progression of 42 cm^{-1} assigned to the perylene twist vibration $1''_u$ marked in red. While the $1a''_u$ vibration changes by 8 cm^{-1} upon complexation in S_1, it changes by 15 cm^{-1} in the S_0 state. The T''_z fundamental is also observed, as well as its combination band with the perylene $1a''_u$. The R''_c fundamental is very weak and lies at 14 cm^{-1}. The intermolecular $''_x$ in-plane overtone and the perylene butterfly $1b''_{1u}$ vibrations are weak but discernible and their assignment agrees with the calculations, as shown in Table 5.

Similar to the R2PI spectrum, the near-origin region of the fluorescence spectrum is essentially repeated in combination with the $1''_g$ mode at $+351$ cm^{-1} (cf. supplementary material). The totally symmetric perylene vibrations $1a''_g$, $2a''_g$ and $3a''_g$ were assigned convincingly as they remain virtually unchanged upon complexation. This is in good agreement with previous findings for the P·2ClE complex.[7] The $3a''_g$ mode shows combination bands with the twist mode as well as the intermolecular stretch, whereas no combination bands involving the $2a''_g$ modes are discernible. The complete assignment of the ground state vibrations is listed in Table 4.

The fluorescence spectrum shows approximate mirror-symmetry to the 2C-R2PI spectrum. The minor differences in intensities can be partly traced to the fact that the R2PI spectrum may still be slightly optically saturated, and partly to the fact that the $1a_u$ and T_z fundamental frequencies are further apart in the S_0 than in the S_1 state, so the harmonic resonance interaction between the two vibrations is smaller in the S_0 state. The medium to small Franck-Condon factors imply that there is little structural change between the **M1** geometries in the S_1 and S_0 states, the two largest changes being with respect to the ω twist angle and the T_z intermolecular stretch. The current assignment of normal mode vibrations is preliminary, as the computational methods differ on the structural changes upon excitation, causing slight disagreement of the Franck-Condon factors. It is

based on excited state observations (2C-R2PI assignment) and a PGOPHER simulation using the ωB97X-D method that is considered the most reliable.[7] We conclude that the dominant progression is caused by the $1a''_u$ vibration. The intensity of the R''_c mode is again strongly overestimated, which is probably due to a very flat potential.

4.3 Perylene·(tetrachloroethene)$_2$

The electronic origin of the P·(4ClE)$_2$ spectrum is observed at 23202 cm^{-1}, shifted by $\delta\nu = -858$ cm^{-1} relative to the perylene origin (24060 cm^{-1}) or by $\delta\nu = -407$ cm^{-1} relative to the P·4ClE origin. The complexation of another tetrachloroethene unit to P·4ClE increases the redshift by a factor of 1.9. The resemblance of the P·4ClE and the P·(4ClE)$_2$ spectra is remarkable. Both observations suggest that we are observing the sandwich-type or 1+1 complex. Topp and coworkers have previously diagnosed the formation of such 1+1 complexes in other perylene complexes with butadiene (factor 1.84),[30] with 1-chlorobutane (1.93)[13] and with benzene (1.87).[13]

Optimizations of sandwich-type P·(4ClE)$_2$ geometries were performed with the B97-D3, M06-2X and ωB97X-D functionals, as discussed in Section 2. Since the two tetrachloroethene molecules on both sides of the perylene chromophore can assume a local **M1**- or **M1'**-geometry, there are two geometrically distinct pairs of degenerate rotamers: The **M1**-top/**M1'**-bottom and **M1'**-top/**M1**-bottom structures are helically (or axially) chiral P/M (or R/S) forms with near D_2 symmetry, whereas the **M1**-top/**M1**-bottom and **M1'**-top/**M1'**-bottom structures are chiral C_2-symmetric *meso*, Figure 13(a) and (b), respectively. In the latter both tetrachloroethene units lie at exactly the same angle, while in the P/M form both units lie at the same angle but in different direction relative to the perylene long axis.

All three methods applied predict the P/M enantiomer, shown in Figure 9, to be the global minimum structure, with both tetrachloroethene units equidistant from the perylene surface at R_{COM}=3.445Å or 6.89 Å apart from each other. The **meso** enantiomer is higher in energy as can be seen from the D_0^{CPC} values in Table 3(ωB97X-D: 105 cm^{-1}. M06-2X: 204 cm^{-1}, B97-D3: 18 cm^{-1}).

S_0 state calculation of the **M1** P/M enantiomer normal-mode frequencies was also performed with the B97-D3, M06-2X and ωB97X-D DFT methods, see Table 6. Note that each rotational (R_i) and translational (T_i) vibration of P·4ClE goes over into a symmetric and asymmetric combination in P·(4ClE)$_2$, giving 12 intermolecular vibrations. To observe the P·(4ClE)$_2$ spectrum, the excitation laser energy had to be raised to $\sim$ 200 μJ/pulse, resulting in saturation of the vibronic bands. Figure 10 shows a preliminary assignment of the observed bands in the low-frequency part of the P·(4ClE)$_2$ spectrum. The assignments are summarized in Table 6 and compared to the corresponding calculated frequencies, which are in good agreement. Note that C_2-symmetry is assumed and only the most prominent excitations are assigned.

5 Discussion

With regard to perylene·tetrachloroethene, Table 5 and Figure 11 (b) show that the B97-D3 method predicts S_0 state harmonic vibrational frequencies that lie very close to the experimental values. The M06-2X, ωB97X-D and SCS-CC2 methods predict higher frequencies than the B97-D3 method, but the differences compared to the experimental values are still acceptable. For the S_1 state the ωB97X-D vibrational frequencies are closest to the experimental values, see Table 5 and Figure 11(a). The frequencies predicted by the M06-2X and M06 functionals lie farther from the experimental ones, with RMSD of 17.9 and 22.2 cm^{-1}, respectively.

Figure 12 compares the experimental $S_0 \rightarrow S_1$ excitation energies to the calculated adiabatic excitation energies of perylene, perylene·*trans*-1,2-dichloroethene[7] and perylene·tetrachloroethene. The M06 method underestimates the perylene $S_0 \rightarrow S_1$ excitation by nearly 3000 cm^{-1}, whereas the spectral shifts of perylene·*trans*-1,2-dichloroethene and perylene·tetrachloroethene relative to perylene are well predicted. The ωB97X-D and M06-2X TD-DFT methods are very close to the experimental $S_0 \rightarrow S_1$ excitation energies. Note that ωB97X-D reproduces the spectral shifts less well than M06-2X, as shown in Figure 12. While SCS-CC2 overestimates the perylene $S_0 \rightarrow S_1$ excitation by $\sim$ 1000 cm^{-1}, the spectral shifts are well predicted.

The elevated background and broad bands in the low-energy part of the 2C-R2PI spectrum is partially due to hot bands and sequence bands from incompletely cooled very low-frequency vibrations, especially the R_c vibrations. As explained in Section 3.1 there are four isomer that are distinguished by the rotation angle ω of tetrachloroethene relative to perylene, and this relative rotation corresponds well to the R_c vibration, see Figure 2.

We studied the intermolecular potential energy curve along the R_c-vibration in more detail. The potential energy curve was calculated with the B97-D3 functional by rotating tetrachloroethene relative to perylene around the c-axis in 5° intervals at a fixed $R_{COM} = 3.423$ Å, as shown in Figure 6. The two global and two local minima correspond to the **M1/M1'** and **M2/M2'** structures discussed above. The barrier heights are upper limits, since they correspond to unrelaxed structures. A potential energy function $V(\theta) = \sum_{i=1}^{n} V_{2n}[1 - cos(2n\theta)]/2$ with $n = 7$ was fitted to the points and the resulting potential scaled by 0.5x to compensate for the lack of structural relaxation at each point. The vibrational eigenvalues were calculated numerically by solving the one-dimensional Schrödinger equation in $V(\theta)$. The reduced mass of 7.5 cm^{-1}/(rad^2) was chosen such that the $v = 1$ level in the **M1** minimum lies 17.7 cm^{-1} above $v = 0$, see Figure 6, thereby reproducing the B97-D3 normal mode R_c harmonic fundamental frequency.

While the potential and vibrational level structure in Figure 6 must be considered qualitative, they show that while the **M1/M1'** minima are narrow, they are not very deep and the barriers towards **M2/M2'** are low. Given the calculated ZPE of 7 cm^{-1}, the R_c $v = 0$ and 1 levels are localized in **M1/M1'**, but the $v = 2, 3$ levels already have amplitude associated with the **M2/M2'** wells and are in fact partially hindered internal-rotation states. Since the barrier between **M2'** and **M2** is similar to that between **M2** and **M1**, the vibrations with $v \geq 4$ are all delocalized over all four minima, i.e., over an angular range of $\sim 150^\circ$. This implies that perylene·tetrachloroethene has only few localized vibrations, and that these are associated with the **M1/M1'** minima. The low barriers for internal rotation along the R_c vibrational coordinate explains why the intensities of the R_c vibrational bands in the experimental spectra are weaker than expected and why these intensities are strongly overestimated in the PGOPHER simulation. In addition, the high density of vibrational

levels at low energies in Figure 6 explains why even at the low vibrational temperatures ($T_{vib} \sim 5-10$K) expected in the supersonic jet, a considerable fraction of the ground-state complexes will be higher vibrational levels $v \geq 2$ that undergo nearly free internal rotation, thereby contributing to the broad background observed in the experiment.

These considerations regarding the R_c potential apply similarly to the P·(4ClE)$_2$ complex, which exhibits an even more dense vibronic features. The increase in the number of vibronic bands in the P·(4ClE)$_2$ spectrum is one hand due to the increased number of intermolecular vibrations (assuming C_2-symmetry), but also due to the increased number of rotational isomers. Besides, the P/M and meso enantiomers with the 4ClE molecules assuming local **M1**- or **M1'**-geometry, the corresponding **M2**-type P/M represent local minima on the potential energy surface. The **M2**-type P/M enantiomer is calculated to be 95 cm^{-1} higher compared to its **M1**-type counterpart with ωB97X-D, 151 cm^{-1} higher with M06-2X and 117 cm^{-1} higher with B97-D3, see D_0^{CPC} in Table 3. The calculations do not predict a **M2** meso enantiomer.

It is noteworthy that the intensity of the T_z' mode is stronger in the P·(4ClE)$_2$ complex, indicating larger structural changes along the complex c-axis, which suggests long-distance interactions between the two acceptors. All methods show an entirely flat perylene subunit in the P·(4ClE)$_2$ *meso* form, indicating that the twisting effect induced in perylene by absorption of one tetrachloroethene is reversed by adsorption of a second 4ClE unit to the other side.

Using the TheoDORE program package of Plasser and Lischka,[31] we calculated the charge-transfer contributionto the $S_0 \rightarrow S_1$ transitions of P·tetrachloroethene and P·1,2-*trans*-dichloroethene,[7] using the transition density matrices of the corresponding SCS-CC2/TZVP calculations. As shown in Figure 14 the CT contribution is indeed small for perylene·1,2-*trans*-dichloroethene, being 0.7%, but it more than doubles to 1.5% in the tetrachloroethene complex . The corresponding charge-density difference plot for perylene·tetrachloroethene, which is included in the Supplemental Material, also show the involvement of the tetrachloroethene subunit. The approximate doubling of the CT contribution from P·2ClE to P·4ClE correlates nicely with the observed $S_0 \rightarrow S_1$ shifts. However, the CT contribution is clearly small, arguing for a "mild" charge transfer.

6 Conclusions

We have measured vibronically well-resolved $S_0 \leftrightarrow S_1$ spectra of the perylene·tetrachloroethene and perylene·(tetrachloroethene)$_2$ clusters, using two-color R2PI and fluorescence spectroscopy in supersonic jets. Structure optimizations in the S_0 and S_1 states were performed using four dispersion-corrected density functionals (B97-D3, M06, M06-2X and ωB97X-D) and the correlated SCS-CC2 method.

All five theoretical methods predict the perylene and tetrachloroethene moieties to be π-stacked and nearly coplanar, with the respective centers of mass of the subunits aligned along the perylene c-axis (surface normal). This is experimentally supported by the observation of strong intermolecular T_z stretching fundamental vibronic bands in the spectra of both perylene·tetrachloroethene and perylene·(tetrachloroethene)$_2$. All methods predict that the intermolecular interaction with tetrachloroethene(s) twists the perylene chromophore around its long axis (x-axis) by $\tau = 3 - 11^\circ$ from its planar D_{2h}-symmetric geometry into a chiral D_2 geometry. This prediction is validated by the appearance of the fundamentals of the $1a_u$ perylene twisting vibration at 42 cm^{-1} (S_0), 55 cm^{-1} (S_1) in perylene·tetrachloroethene and at 52 cm^{-1} in the S_1 state of perylene·(tetrachloroethene)$_2$.

All methods except M06 predict two chiral minimum-energy structures of perylene·tetrachloroethene, denoted **M1/M1'** and **M2/M2'**, in which the subunits are mutually rotated around the perylene c-axis by angles of $\omega \sim \pm 60^\circ$ and $\omega \sim \pm 25^\circ$. The existence of four rotamers implies a large internal-rotation mobility of perylene·tetrachloroethene. The intermolecular potential energy curve was calculated along ω. The vibrations calculated in this potential are localized in the **M1** well only for $v = 0$ and 1. The levels $v = 2 - 4$ are partially or fully delocalized over the **M1/M2/M2'/M1'** minima and are split by tunneling. For $v \geq 5$ the wave functions correspond to essentially free internal rotation. This is experimentally supported by the observation of narrow and well-resolved vibronic bands which are superimposed on broad-band structures in the same spectral region. The sharp vibronic bands are assigned to complexes that are localized in the $v = 0$ level of the **M1/M1'** minima. The slightly structured broad bands correspond to complexes in $v \geq 2$ levels that are partially or fully delocalized over the internal-rotational coordinate.

The $S_0 \rightarrow S_1$ 0_0^0 band of perylene·tetrachloroethene is redshifted by $\delta\nu = -451$ cm^{-1} relative to perylene, corresponding to an increase of D_0 by 5.4 kJ/mol. Given that the M06-2X, ωB97X-D and B97-D3 calculated S_0 state dissociation energies are $D_0 = 28 - 35$ kJ/mol, this corresponds to an increase by $15 - 19$ %, in agreement with the mild charge-transfer character of the complex. The redshift of perylene·tetrachloroethene is $\sim 30\%$ larger than that of perylene·*trans*-1,2-dichloroethene, so the increase in chlorination increases the excited-state stabilization and charge-transfer character of the excitation.

The DFT calculations predict perylene·(tetrachloroethene)$_2$ to be the π-stacked sandwich or (1+1) cluster with four different minimum-energy forms, namely the chiral plus/minus (P/M) and achiral *meso* isomers of **M1**-type and **M2**-type; the **M1**-type P/M rotamer is predicted to be the most stable. The increased number of rotational isomers is experimentally supported by the vibronic spectrum of perylene·(tetrachloroethene)$_2$, which exhibits more intense broad-band features and approximately twice the number of vibronic bands as perylene·tetrachloroethene. Its $S_0 \rightarrow S_1$ redshift is $\delta\nu = -858$ cm^{-1} relative to perylene, corresponding to a dissociation energy increase of 10.3 kJ/mol, or of 1.90 times that of perylene·tetrachloroethene. The calculated S_0 state dissociation energies of perylene·(tetrachloroethene)$_2$ are $2.03 - 2.04$ times that of perylene·tetrachloroethene (see Table 3), indicating a small stabilizing three-body interaction on the ground state. In contrast, the smaller than twofold spectral redshift indicates that the S_1 state is *de*stabilized by the three-body interaction.

The theoretical methods were benchmarked against the experimental data on perylene·tetrachloroethene. The adiabatic $S_0 \rightarrow S_1$ excitation energies and vibrational frequencies predicted by the M06-2X and ωB97X-D DFT methods are closer to experiment than those of M06. For the S_0 state frequencies, the B97-D3 method shows the best agreement with experiment. These findings are similar to those for perylene·1,2-dichloroethene.[7] The M06-2X, ωB97X-D and B97-D3 calculations predict counterpoise-corrected dissociation energies between $D_0^{CPC} = 28.8$ and 37.5 kJ/mol. The SCS-CC2 method suffers from a large BSSE even with the large def2-QZVPP basis set, which leads to a counterpoise overcorrection and a too small D_0^{CPC}. The calculated spectral red shifts relative to

bare perylene, which correspond to the increase in the calculated D_0^{CPC} upon $S_0 \rightarrow S_1$ excitation, are about half the observed shift. This indicates that the theoretical treatment of the excited state needs to be improved. The $S_0 \rightarrow S_1$ adiabatic excitation energy predicted by M06 for perylene is ~ 3000 cm^{-1} too low, that predicted with the SCS-CC2 method is about 1000 cm^{-1} too high. However, for both methods the difference relative to the experimental values is nearly constant for perylene, perylene·1,2-dichloroethene and perylene·tetrachloroethene.

Acknowledgments

This work was supported by the Schweiz. Nationalfonds (project 200020-121993).

Supporting Information

Figure S1 with definition of the structure parameters of perylene·tetrachloroethene, Table S1 and S2 with the S_0 state and S_1 state B97-D3, M06, M06-2X, ωB97X-D and SCS-CC2 calculated structure parameters of perylene·tetrachloroethene. Tables III to V with calculated Cartesian coordinates, Figure 2 with the twelve intermolecular vibrations of perylene·(tetrachloroethene)$_2$, Figure 3 with higher-frequency part of the dispersed fluorescence spectra of the perylene·tetrachloroethene.

References

(1) Mulliken, R. Molecular Compounds and Their Spectra. II. *J. Am. Chem. Soc.* **1952**, *74*, 811–824.

(2) Mulliken, R. Molecular Compounds and Their Spectra. III. The Interaction of Electron Donors and Acceptors. *J. Phys. Chem.* **1952**, *56*, 801–822.

(3) Russell, T.; Levy, D. Fluorescence Spectrum of the Charge-Transfer Complex Tetracyanoethylene-para-Xylene Cooled in a Supersonic Free Jet. *J. Phys. Chem.* **1982**, *86*, 2718–2727.

(4) Foster, R. Electron Donor-Acceptor Complexes. *J. Phys. Chem.* **1980**, *84*, 2135–2141.

(5) Cozzi, F.; Cinquini, M.; Annuziata, R.; Siegel, J. Dominance of Polar/π over Charge-Transfer Effects in Stacked Phenyl Interactions. *J. Am. Chem. Soc.* **1993**, *115*, 5330–5331.

(6) Shchuka, M. I.; Motyka, A. L.; Topp, M. R. 2-Photon Threshold Ionization Spectroscopy of Perylene and van der Waals Complexes. *Chem. Phys. Lett* **1989**, *164*, 87–95.

(7) Balmer, F. A.; Ottiger, P.; Pfaffen, C.; Leutwyler, S. Structure and Intermolecular Vibrations of Perylene·*trans*-1,2-Dichloroethene, a Weak Charge-Transfer Complex. *J. Phys. Chem. A* **2013**, *117*, 10702–10713.

(8) Bouzou, C.; Jouvet, C.; Leblond, J. B.; Millié, P.; Tramer, A. Vibrational Redistribution in Jet-Cooled Perylene. Intermediate Coupling Case. *Chem. Phys. Lett.* **1983**, *97*, 161–166.

(9) Leutwyler, S. Electronic Spectroscopy of Perylene-Rare-Gas van der Waals Complexes. *J. Chem. Phys.* **1984**, *81*, 5480–5493.

(10) Fourmann, B.; Jouvet, C.; Tramer, A.; LeBars, J.; Millié, P. Fluorescence Spectra and Intramolecular Vibrational Redistribution in Jet-Cooled Perylene. *Chem. Phys.* **1985**, *92*, 25–42.

(11) Fillaux, F. Butterfly Motion of Isolated Perylene in its Ground and First Excited Singlet States. *Chem. Phys. Lett.* **1985**, *114*, 384–387.

(12) Babbitt, R.; Doxtader, M.; Bhattacharya, A.; Topp, M. Jet Spectroscopy of Perylene Complexes: Comparisons of TMS, Carbon Dioxide, Ethylene and Butadiene. *Chem. Phys.* **1987**, *113*, 405–416.

(13) Wittmeyer, S.; Topp, M. Spectral Hole Burning in Free Perylene and in Small Clusters with Methane and Alkyl Halides. *Chem. Phys. Lett.* **1989**, *163*, 261–268.

(14) Tan, X.; Salama, F. Cavity Ring-Down Spectroscopy and Theoretical Calculations of the $S_1(^1B_{3u}) \leftarrow S_0(^1A_g)$ Transition of Jet-Cooled Perylene. *J. Chem. Phys.* **2005**, *122*, 084318–1 – 084318–9.

(15) Suganuma, Y.; Kowaka, Y.; Ashizawa, N.; Nakayama, N.; Goto, H.; Ishimoto, T.; Nagashima, U.; Ueda, T.; Yamanaka, N., T. Nishi; Baba, M. Mode-selective Internal Conversion of Perylene. *Mol. Phys.* **2011**, *109*, 1831–1840.

(16) Burrow, P.; Modelli, A.; Chiu, N.; Jordan, K. Temporary Σ and Π Anions of the Chloroethylenes and Chlorofluoroethylenes. *Chem. Phys. Lett.* **1981**, *82*, 270–276.

(17) Dreuw, A.; Weisman, J. L.; Head-Gordon, M. Long-Range Charge-Transfer Excited States in Time-Dependent Density Functional Theory Require Nonlocal Exchange. *J. Chem. Phys.* **2003**, *119*, 2943–2946.

(18) Zhao, Y.; Truhlar, D. G. The M06 Suite of Density Functionals for Main Group Thermochemistry, Thermochemical Kinetics, Noncovalent Interactions, Excited States, and Transition Elements. *Theor. Chem. Accts.* **2008**, *120*, 215–241.

(19) Grimme, S. Accurate Description of van der Waals Complexes by Density Functional Theory including Empirical Corrections. *J. Comput. Chem.* **2004**, *25*, 1463–1473.

(20) Chai, J.-D.; Head-Gordon, M. Long-range Corrected Hybrid Density Functionals with Damped Atom-Atom Dispersion Corrections. *Phys. Chem. Chem. Phys.* **2008**, *10*, 6615–6620.

(21) Hill, J. G.; Platts, J. A.; Werner, H.-J. Calculation of Intermolecular Interactions in the Benzene Dimer using Coupled-cluster and Local Correlation Methods. *Phys. Chem. Chem. Phys.* **2006**, *8*, 4072–4078.

(22) Leist, R.; Frey, J. A.; Ottiger, P.; Frey, H. M.; Leutwyler, S.; Bachorz, R. A.; Klopper, W.

Nucleobase-Fluorobenzene Interactions: Hydrogen Bonding Wins over pi-Stacking. *Angew. Chem. Int. Ed.* **2007**, *46*, 7449–7452.

(23) Bachorz, R. A.; Bischoff, F. A.; Höfener, S.; Klopper, W.; Ottiger, P.; Leist, R.; Frey, J. A.; Leutwyler, S. Scope and Limitations of the SCS-MP2 Method for Stacking and Hydrogen Bonding Interactions. *Phys. Chem. Chem. Phys.* **2008**, *10*, 2758–2766.

(24) Boys, S. F.; Bernardi, F. Calculation of Small Molecular Interactions by Differences of Separate Total Energies - Some Procedures with Reduced Errors. *Mol. Phys.* **1970**, *19*, 553–561.

(25) TURBOMOLE *V6.3 2011*; a development of Universität Karlsruhe (TH) and Forschungszentrum Karlsruhe GmbH, 1989-2007, TURBOMOLE GmbH; available from `http://www.turbomole.com`.

(26) Frisch, M. J.; Trucks, G. W.; Schlegel, H. B.; Scuseria, G. E.; Robb, M. A.; Cheeseman, J. R.; Scalmani, G.; Barone, V.; Mennucci, B.; Petersson, G. A.; et al., Gaussian 09 Revision A.1. Gaussian Inc. Wallingford CT 2009.

(27) Grimme, S. Semiempirical GGA-Type Density Functional Constructed with a Long-Range Dispersion Correction. *J. Comput. Chem.* **2006**, *27*, 1787–1799.

(28) Kaziska, A. J.; Wittmeyer, S. A.; Topp, M. R. Picosecond Time Resolution of Vibrational-Relaxation in Molecular van der Waals Complexes: Perylene with Naphthalene and Benzene. *J. Phys. Chem.* **1991**, *95*, 3663–3670.

(29) Western, C. M. *PGOPHER 7.0, a Program for Simulating Rotational, Vibrational and Electronic Structure*; 2013; pgopher.chm.bris.ac.uk.

(30) Doxtader, M.; Topp, M. Structure and Dynamics of Perylene Complexes: Comparisons of Atomic and Molecular Complexation. *Chem. Phys.* **1987**, *113*, 405–416.

(31) Plasser, F.; Lischka, H. Analysis of Excitonic and Charge Transfer Interactions from Quantum Chemical Calculations. *J. Chem. Theory Comput.* **2012**, *8*, 2777–2789.

Table 1: Experimental and Calculated Adiabatic and Vertical Electron Affinities of Chloroethenes (in eV).

Acceptor	B97-D3 def2-TZVPP adiabatic	SCS-MP2 aug-cc-pVTZ adiabatic	Experimental vertical [a]	Experimental adiabatic [b]
Ethene	-2.10	-1.74	-1.73	
Chloroethene	-1.62	-1.38	-1.28	
trans-1,2-Dichloroethene	-1.17	-1.06	-0.80	
Trichloroethene	-0.90	-0.93	-0.59	-0.40±0.22
Tetrachloroethene	-0.61	-0.78	-0.30	-0.64±0.03

a From ref. 16.

Table 2: Structure Parameters of the Minima **M1** and **M2** of Perylene·Tetrachloroethene and Perylene·(Tetrachloroethene)$_2$.

P·4ClE **M1**	M06	M06-2X	B97-D3	ωB97X-D	SCS-CC2
$R_{COM}(S_0)$	3.434 Å	3.339 Å	3.423 Å	3.476 Å	3.350 Å[a]
$R_{COM}(S_1)$	3.406 Å	3.295 Å	–	3.442 Å	3.287 Å[a]
$\omega(S_0)$	45.8°	59.6°	58.7°	56.6°	58.7°
$\omega(S_1)$	43.9°	62.7°	–	62.1°	59.6°
$\tau(S_0)$	2.9°	6.8°	5.5°	5.5°	11.1°
$\tau(S_1)$	1.6°	3.0°	–	1.9°	6.2°
P·4ClE **M2**					
$R_{COM}(S_0)$	–	3.346 Å	3.439 Å	3.489 Å	3.353 Å[a]
$R_{COM}(S_1)$	–	3.134 Å	–	3.449 Å	3.284 Å[a]
$\omega(S_0)$	–	21.6°	19.7°	23.3°	30.7°
$\omega(S_1)$	–	25.3°	–	23.7°	31.8°
$\tau(S_0)$	–	8.9°	7.3°	7.3°	8.8°
$\tau(S_1)$	–	4.4°	–	2.7°	8.5°
P·(4ClE)$_2$ **M1** P/M					
$R_{COM}(S_0)$	–	3.330 Å	3.427 Å	3.469 Å	–
$\omega(S_0)$	–	$\pm$61.2°	$\pm$59.7°	$\pm$60.4°	–
τ (Perylene)	–	8.1°	6.5°	6.9°	–
P·(4ClE)$_2$ **M1** *meso* form					
$R_{COM}(S_0)$	–	3.329 Å	3.427 Å	3.466Å	–
$\omega(S_0)$	–	$\pm$59.7°	$\pm$57.5°	$\pm$56.6°	–
τ (Perylene)	–	0.0°	0.0°	0.0°	–
P·(4ClE)$_2$ **M2** P/M					
$R_{COM}(S_0)$	–	3.333 Å	3.443 Å	3.475Å	–
$\omega(S_0)$	–	$\pm$24.4°	$\pm$23.5°	$\pm$26.2°	–
τ (Perylene)	–	10.4°	8.3°	8.7°	–

a re-optimized with the def2-TZVPP basis set, see the text.

Table 3: Calculated Binding Energies D_e, Dissociation Energies D_0 and Basis-Set Superposition Errors (BSSE) of the Perylene·Tetrachloroethene **M1** and **M2** Structures in the S_0 and S_1 States, and Perylene·(Tetrachloroethene)$_2$ in the S_0 state (in kJ/mol).

	$\mathbf{S_0}$		$\mathbf{S_1}$	
P·4ClE **M1**	$-D_e^{CPC}(BSSE)$	$-D_0^{CPC}$	$-D_e^{CPC}(BSSE)$	$-D_0^{CPC}$
B97-D3	37.45[a]	35.11 [a]	–	–
M06	31.30 (8.59)	28.75	32.89 (10.17)	31.39
M06-2X	35.60 (6.95)	32.76	39.80 (8.45)	35.20
ωB97X-D	34.42 (7.37)	31.78	37.08 (8.34)	33.89
SCS-CC2/TZVP	11.60 (56.41)	9.18	15.32 (61.45)	12.68[b]
SCS-CC2/def2-TZVPP	20.54 (20.16)	18.12 [c]	–	–
SCS-CC2/QZVP	46.94 (8.18)	– –	–	
P·4ClE **M2**	$-D_e^{CPC}(BSSE)$	$-D_0^{CPC}$	$-D_e^{CPC}(BSSE)$	$-D_0^{CPC}$
B97-D3	36.66[a]	34.41 [a]	–	–
M06-2X	34.53 (6.95)	31.94	39.62 (8.08)	34.97
ωB97X-D	33.11 (8.08)	29.92	36.98 (8.16)	34.03
SCS-CC2/TZVP	11.53 (56.59)	8.93	15.83 (60.34)	–
SCS-CC2/def2-TZVPP	19.79 (20.09)	–	–	–
P·(4ClE)$_2$ **M1** P/M	$-D_e^{CPC}(BSSE)$	$-D_0^{CPC}$		
B97-D3	75.78[a]	71.46[a]		
M06-2X	72.09 (14.12)	66.97		
ωB97X-D	70.16 (15.03)	63.83		
P·(4ClE)$_2$ **M1** *meso*-form	$-D_e^{CPC}(BSSE)$	$-D_0^{CPC}$		
B97-D3	74.70[a]	71.24[a]		
M06-2X	68.63 (14.09)	64.53		
ωB97X-D	67.02 (14.90)	62.58		
P·(4ClE)$_2$ **M2** P/M	$-D_e^{CPC}(BSSE)$	$-D_0^{CPC}$		
B97-D3	74.38[a]	70.33[a]		
M06-2X	70.01 (14.23)	65.16		
ωB97X-D	68.63 (15.42)	62.43		

a Counterpoise correction is not recommended for the B97-D3 method.[27]
b Zero-point vibrational energy corrected at the ωB97X-D level.
c Zero-point vibrational energy corrected at the SCS-CC2/TZVP level.

Table 4: Experimental Perylene·Tetrachloroethene S_0 and S_1 State Vibrational Frequencies (in cm^{-1}).

Assignment S_0	Fluorescence	Assignment S_1	2C-R2PI
0_0^0	(23609)	$(R_c)_1^0$	-12.8
$(R_c)_1^0$	13	$(R_c)_1^1$	-2.8
$(R_c)_2^0$	27	0_0^0	(23609)
$(1a_u)_1^0$	42	$(T_z)_1^1$	5.6
$(T_z)_1^0$	55	$(R_c)_2^1$	7.9
$(T_x)_2^0$	60	$(R_c)_0^1$	10.9
$(1a_u)_2^0$	83	$(R_c)_0^2$	21.8
$(1a_u)_2^0(R_c)_1^0$	97	$(1a_u)_0^1(R_c)_1^0$	41.7
$(1a_u)_1^0(T_z)_1^0$	99	$(T_z)_0^1(R_c)_1^0$	46.3
$(1b_{1u})_1^0$	101	$(T_x)_0^2(R_c)_1^0$	50.5
$(1a_u)_1^0(T_x)_2^0$	103	$(1a_u)_0^1$	55.3
$(1a_g)_1^0$	352	$(T_z)_0^1$	60.2
$(1a_g)_1^0(R_c)_1^0$	365	$(T_x)_0^2$	64.1
$(1a_g)_1^0(R_c)_2^0$	376	$(1b_{1u})_0^1$	95.1
$(1a_g)_1^0(1a_u)_1^0$	394	$(1a_u)_0^2$	111.0
$(1a_g)_1^0(T_z)_1^0$	407	$(1a_u)_0^1(T_z)_0^1$	115.5
$(1a_g)_1^0(T_x)_2^0$	412	$(T_z)_0^2$	118.8
$(2a_g)_1^0$	426	$(1a_u)_0^1(1b_{1u})_0^1$	149.9
$(1a_g)_1^0(1a_u)_2^0$	434	$(1a_g)_1^0(1a_u)_1^0(T_z)_1^0$	450
$(3a_g)_1^0$	547	$(1a_u)_0^3$	167.1
$(1a_g)_1^0(2a_u)_1^0$	548	$(1a_u)_0^2(T_z)_0^1$	171.1
$(3a_g)_1^0(1a_u)_1^0$	586	$(1a_u)_0^1(T_z)_0^2$	174.2
		$(T_z)_0^3$	196.7

Continued on next page

Table 4 – continued from previous page

Assignment S_0	Fluorescence	Assignment S_1	2C-R2PI
		$(2a_u)^1_0$	200.0
		$(1a_u)^4_0$	223.4
		$(1a_g)^1_0$	351.3
		$(1a_g)^1_0(R_c)^1_0$	362.8
		$(1a_g)^1_0(1a_u)^1_0$	406.2
		$(1a_g)^1_0(T_z)^1_0$	411.5
		$(1a_g)^1_0(T_x)^2_0$	415.8
		$(2a_g)^1_0$	425.7
		$(1a_g)^1_0(1a_u)^2_0$	461.5
		$(1a_g)^1_0(1a_u)^1_0(T_z)^1_0$	466.4
		$(2a_g)^1_0(1a_u)^1_0$	478.6
		$(1a_g)^1_0(1a_u)^3_0$	516.7
		$(3a_g)^1_0$	542.0
		$(1a_g)^1_0(2a_u)^1_0$	551.3
		$(3a_g)^1_0(1a_u)^1_0$	597.2
		$(3a_g)^1_0(T_z)^1_0$	602.9
		$(1a_g)^1_0(1a_u)^1_0(2a_u)^1_0$	606.2
		$(1a_g)^1_0(T_z)^1_0(2a_u)^1_0$	611.4

Table 5: Experimental and Calculated S_0 and S_1 Vibrational Frequencies (in cm^{-1}) of the Perylene·Tetrachloroethene **M1** Isomer.

Vibration	S_0 state	B97-D3 def2-TZVPP	M06 6-31++G(d,p)	SCS-CC2 TZVP	M06-2X 6-31++G(d,p)	ωB97X-D 6-31++G(d,p)
T_y		14.7	44.2	30.8	22.8	20.8
R_c	14	17.7	22.8	25.9	18.2	17.5
T_x	30	30.8	16.9	42.9	39.2	33.6
$1a_u$	42	37.9	50.2	58.9	49.4	41.1
R_a		52.2	79.6	75.1	65.7	66.0
T_z	56	61.9	72.6	84.3	74.8	77.3
R_b		65.3	57.7	92.5	74.8	83.1
$1b_{1u}$	101	99.7	99.0	109.9	109.3	109.8
$2a_u$	197	230.4	238.0	243.9	232.6	243.4
$1a_g$	352	351.1	358.9	350.7	358.9	358.8
$2a_g$	426	430.6	435.5	449.8	433.1	438.8
$3a_g$	546	546.0	559.2	552.2	560.7	561.6
RMSD [a]	-	11.6	17.0	17.6	18.4	18.9
	S_1 state					
R_c	10.9		30.9		28.7	16.9
T_x	32.05		19.8		32.8	25.1
T_y			54.1		45.8	35.8
$1a_u$	55.3		71.1		69.9	65.7
R_a			83.6		90.5	70.2
T_z	60.2		103.5		78.1	72.7
R_b			74.6		85.3	82.9
$1b_{1u}$	95.1		77.1		116.8	104.6
$2a_u$	200.0		229.0		225.9	222.1
$1a_g$	351.3		368.1		370.2	371.8
$2a_g$	425.7		437.5		443.2	446.7
$3a_g$	542.0		555.8		557.7	558.9
RMSD [a]	-		22.2		17.9	15.2

a Root-mean-square deviation between calculated and experimental wavenumber.

Table 6: Experimental and Calculated Vibrational Frequencies of the Perylene·(Tetrachloroethene)$_2$ P/M Isomer.

Vibration	S_1 state	M06-2X	ωB97X-D	B97-D3
$R_{c,s}$	9.3	12.7	22.3	13.6
$T_{y,as}$		15.6	19.9	15.9
$R_{c,as}$	11.3	18.0	25.1	16.2
$T_{y,s}$		24.5	31.4	22.4
$T_{x,as}$		37.1	34.1	27.9
$T_{x,s}$		40.7	36.8	29.5
$R_{a,as}$		57.3	62.5	47.9
$1a_u$	51.6	60.4	59.8	55.9
$T_{z,s}$	61.1	64.5	78.3	47.7
$R_{b,as}$		66.2	69.2	50.4
$R_{a,s}$		72.8	96.3	63.3
$R_{b,s}$		75.6	93.2	64.0
$T_{z,as}$	48.8	79.5	85.4	69.6

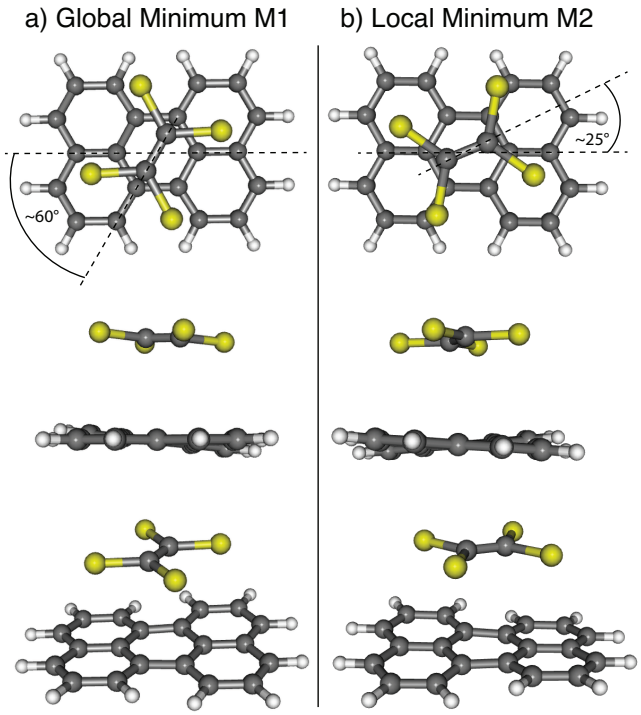

Figure 1: S_0 state structures of perylene·tetrachloroethene, calculated with the ωB97X-D density functional. (a) Global minimum **M1**, (b) local minimum **M2**. The views shown are along the c-axis (top), along the a-axis (middle) and general (bottom).

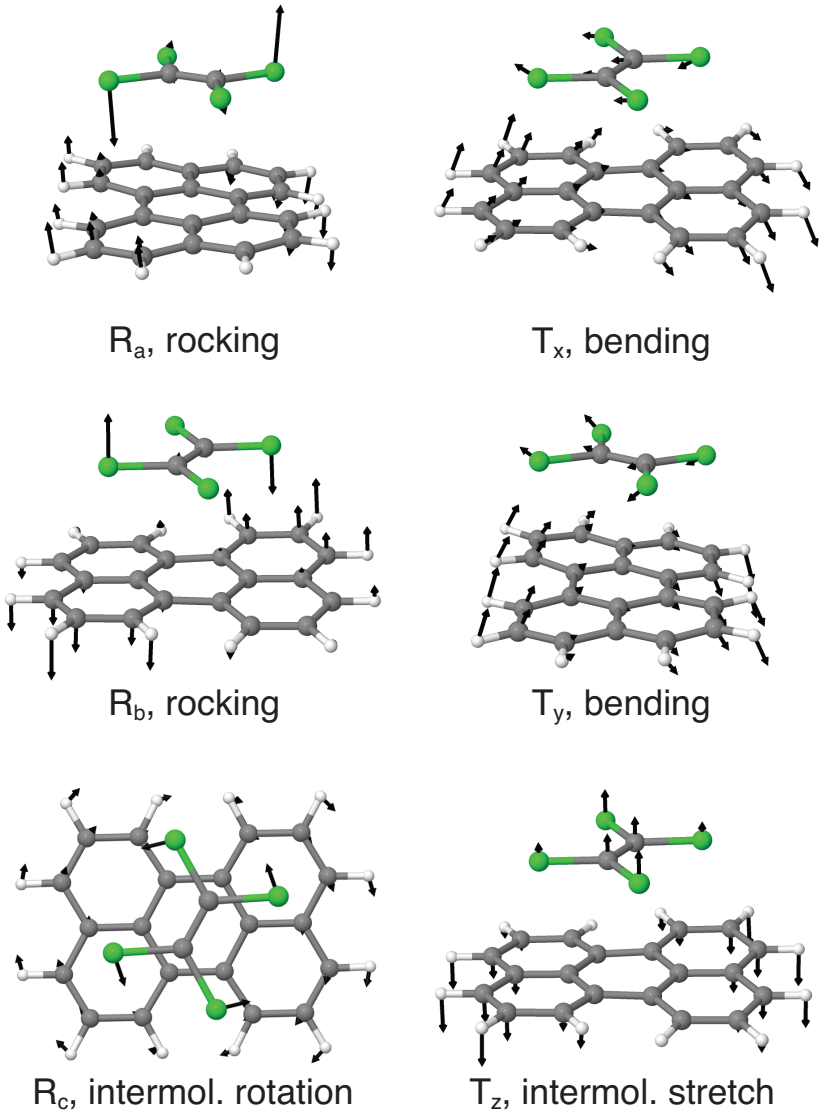

Figure 2: Intermolecular normal-mode eigenvectors of the intermolecular vibrations of perylene·tetrachloroethene, (T_i: hindered translational modes, R_i: hindered internal-rotation modes).

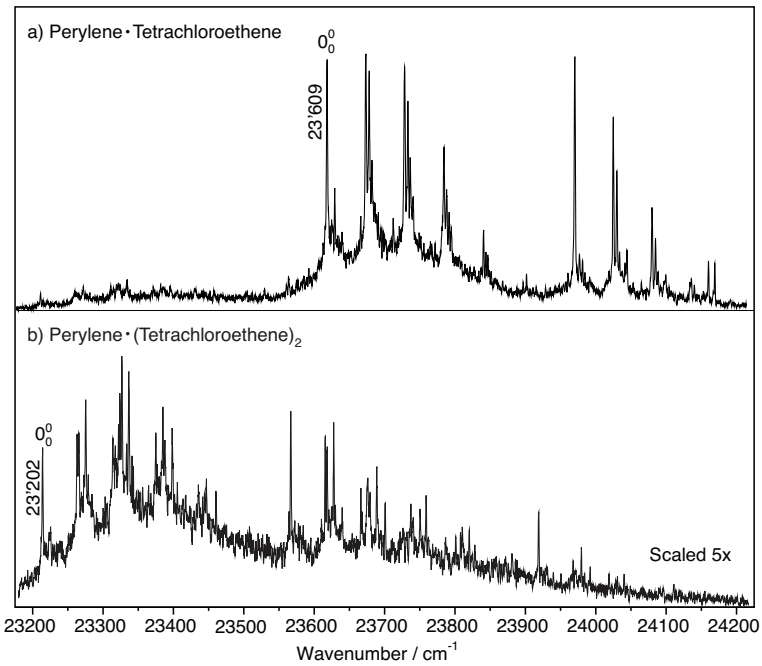

Figure 3: Two-color resonant two-photon ionization (2C-R2PI) spectra of (a) perylene·tetrachloroethene and (b) perylene·(tetrachloroethene)$_2$. The spectra were recorded simultaneously, at an excitation laser pulse energy of 200 μJ/pulse. The ion signal of (b) is scaled 5x relative to (a).

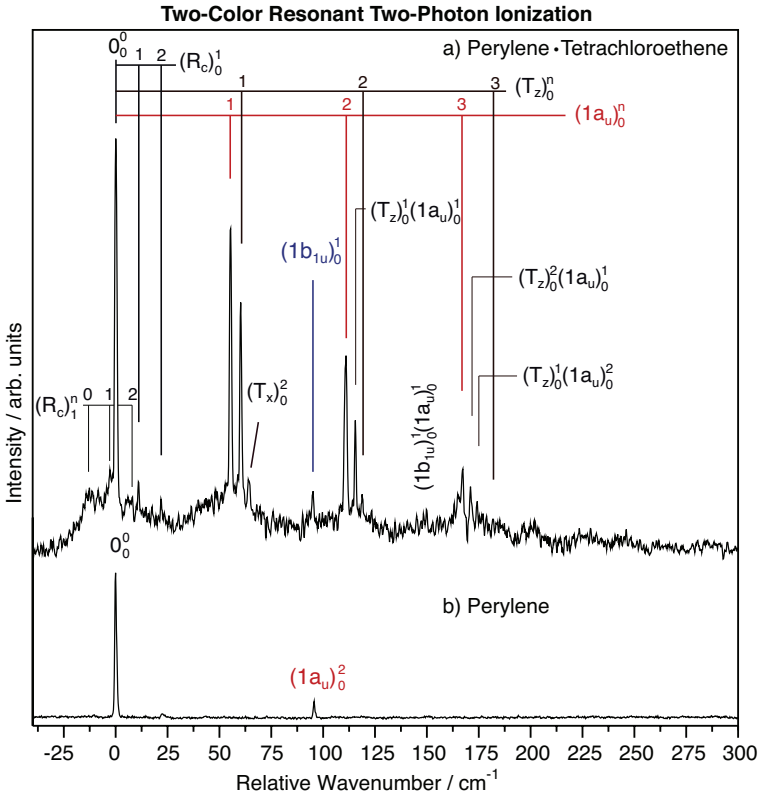

Figure 4: Low-frequency region of the 2C-R2PI spectra of (a) perylene·tetrachloroethene and (b) bare perylene (in cm^{-1}, relative to the 0_0^0 band), with band assignments, at excitation laser 20 μJ/pulse energy. Perylene intramolecular $1a_u$ and $1b_{1u}$ out-of-plane excitations are indicated in red and blue, respectively.

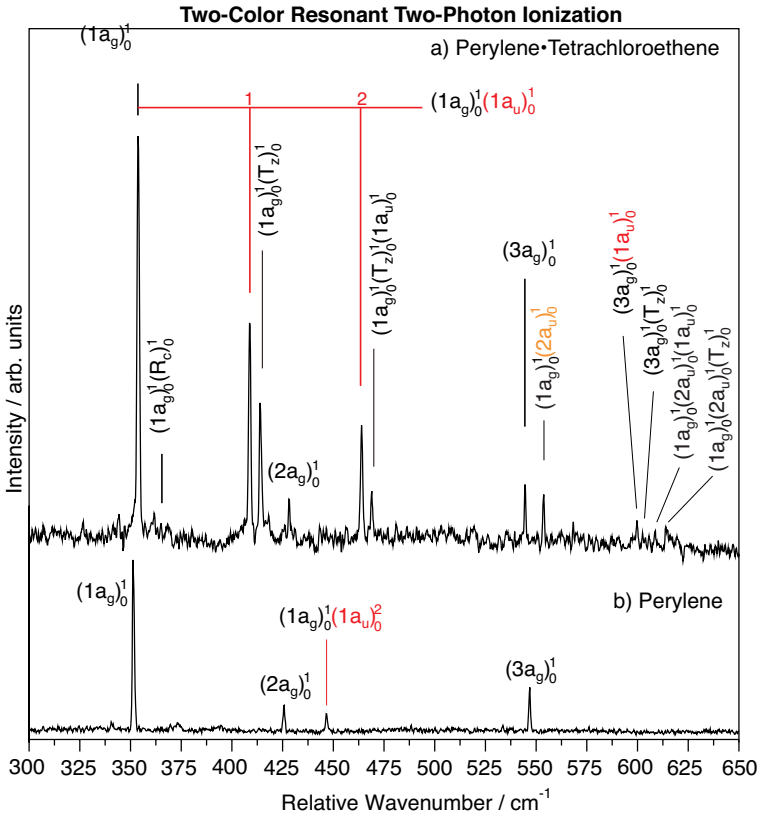

Figure 5: High-frequency part of the 2C-R2PI spectra of (a) perylene·tetrachloroethene and (b) perylene (in cm^{-1}, relative to the 0_0^0 band) with band assignments. The full assignments are listed in Table 4. Perylene out-of-plane $1a_u$ and $2a_u$ excitations marked in red and orange, respectively.

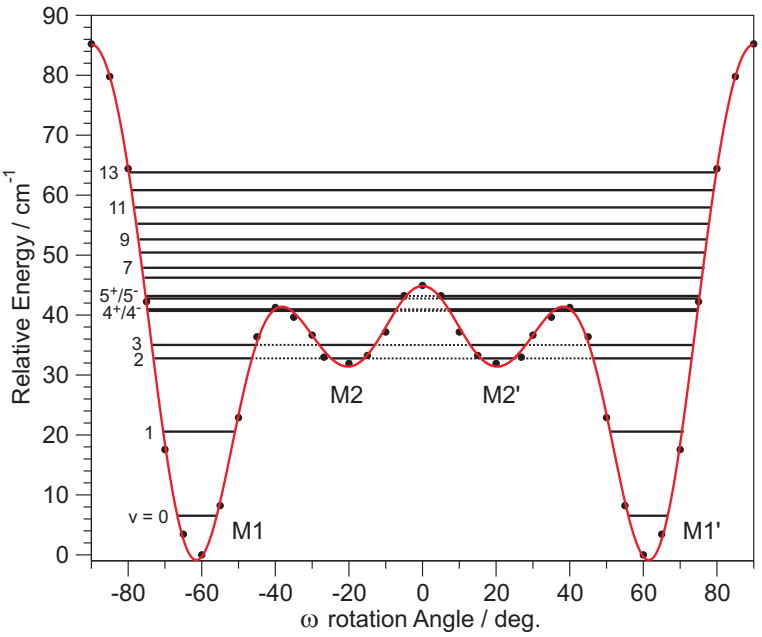

Figure 6: Potential energy curve calculated along the intermolecular rotational angle ω; $\omega = 0^\circ = 180^\circ$ is defined as in Figure 1. The anharmonically calculated vibrational levels (see the text) are drawn as horizontal lines.

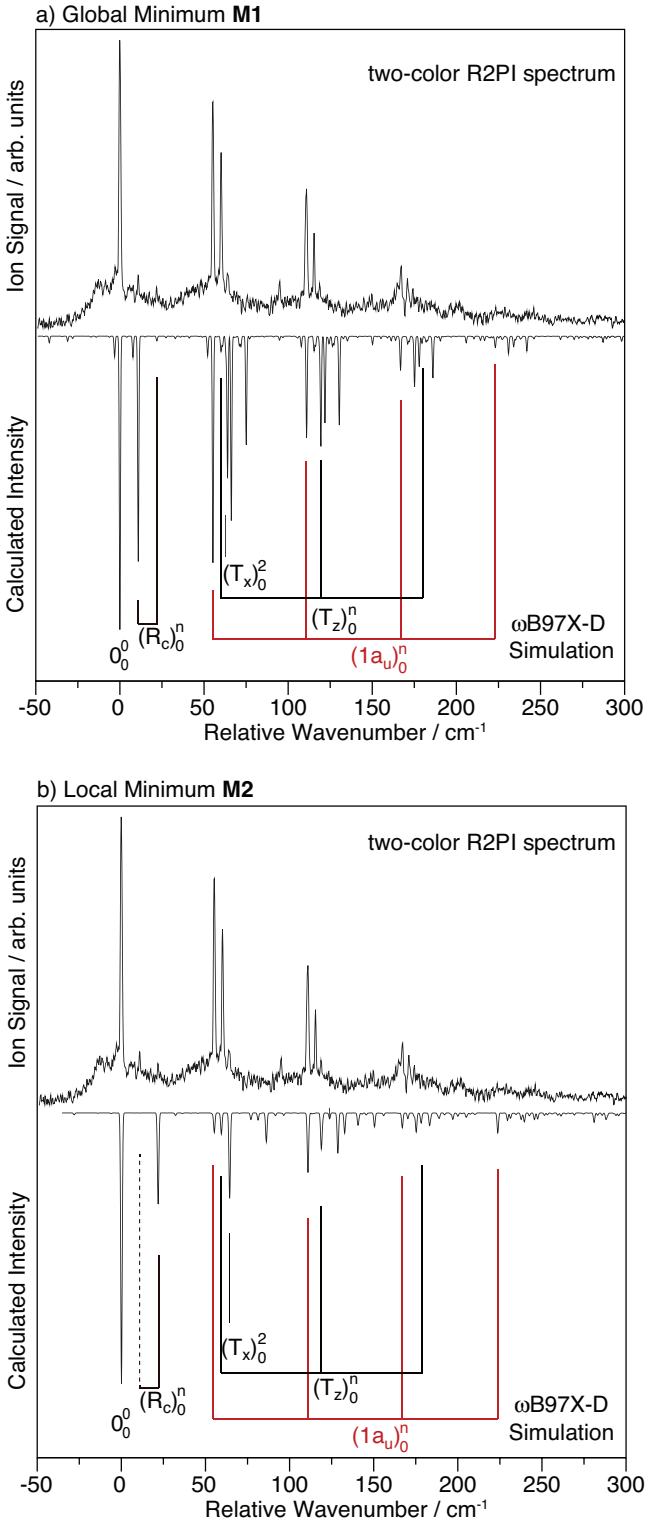

Figure 7: Comparison of 2C-R2PI spectrum of perylene·tetrachloroethene (Figure 4a) to PGOPHER vibronic simulations based on the ωB97X-D calculated S_0 and S_1 state geometries and normal modes for (a) the global minimum **M1** and (b) the local minimum **M2**.

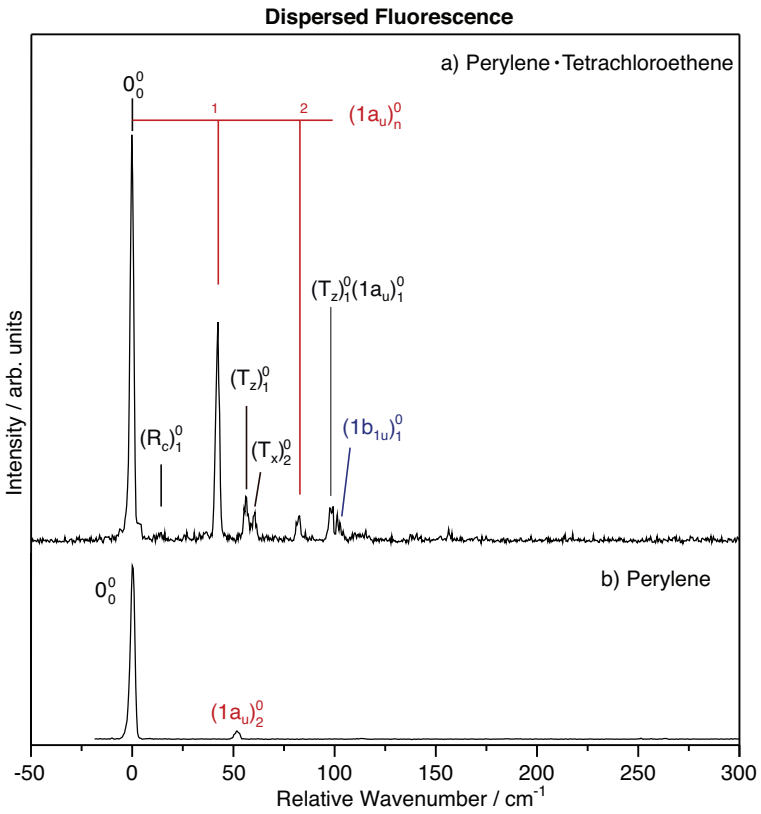

Figure 8: Dispersed fluorescence spectra of (a) perylene·tetrachloroethene and (b) perylene (in cm^{-1}, relative to the respective 0_0^0 band) with assignments (see also Table 4). The perylene-localized out-of-plane $1a_u$ and $1b_{1u}$ excitations are marked in red and blue.

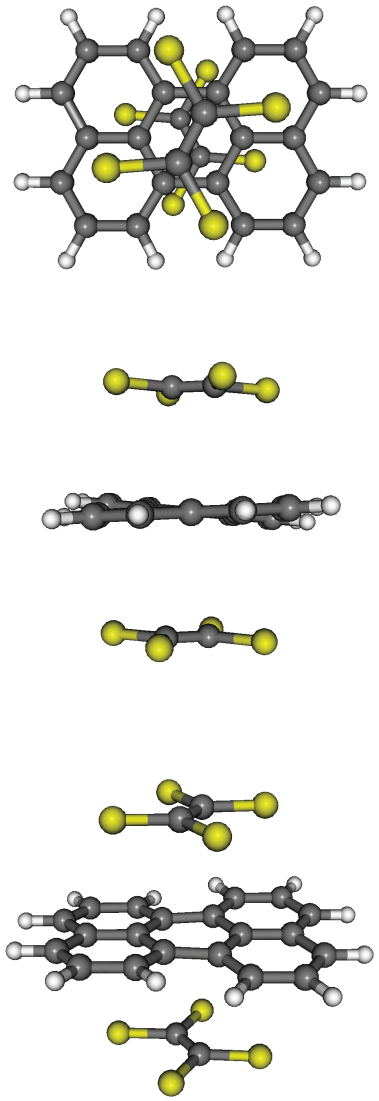

Figure 9: Calculated structure of perylene·(tetrachloroethene)$_2$ (ωB97X-D) in the M1/M1' conformation. Views are along the c-axis (top), along the x-axis (middle), general view (bottom).

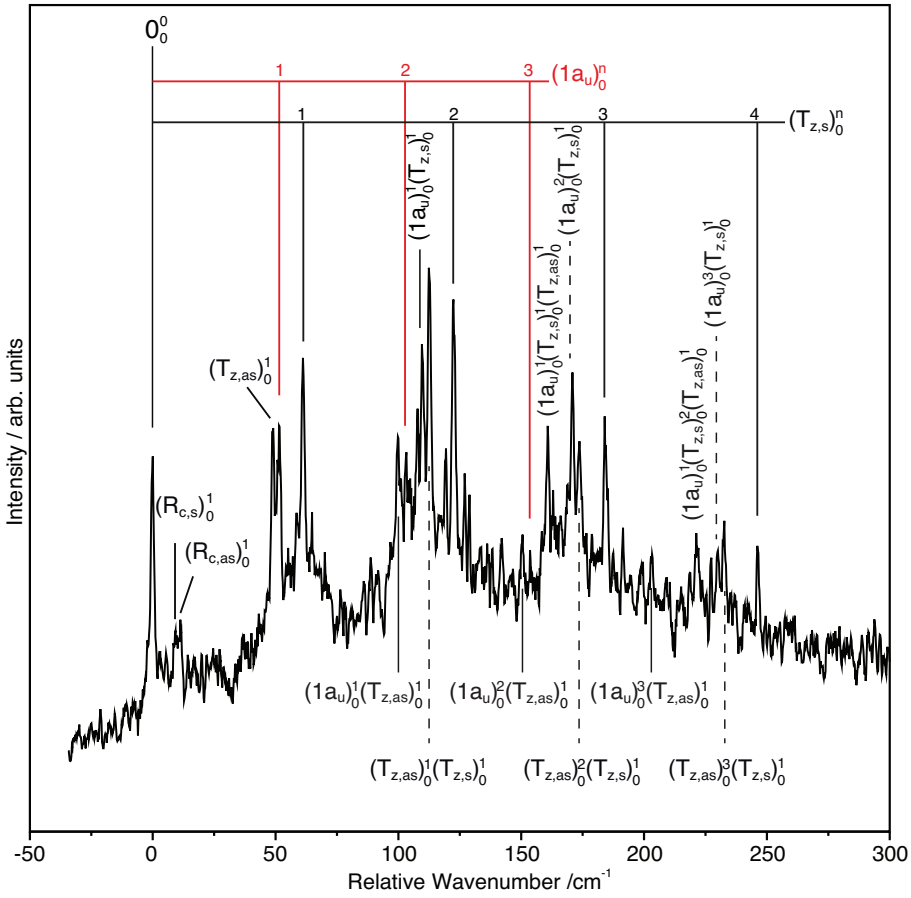

Figure 10: Low-energy region of the 2C-R2PI spectrum of perylene·$(4ClE)_2$ 2C-R2PI with assignments. The perylene intramolecular twist $1a_u$ excitations are marked in red.

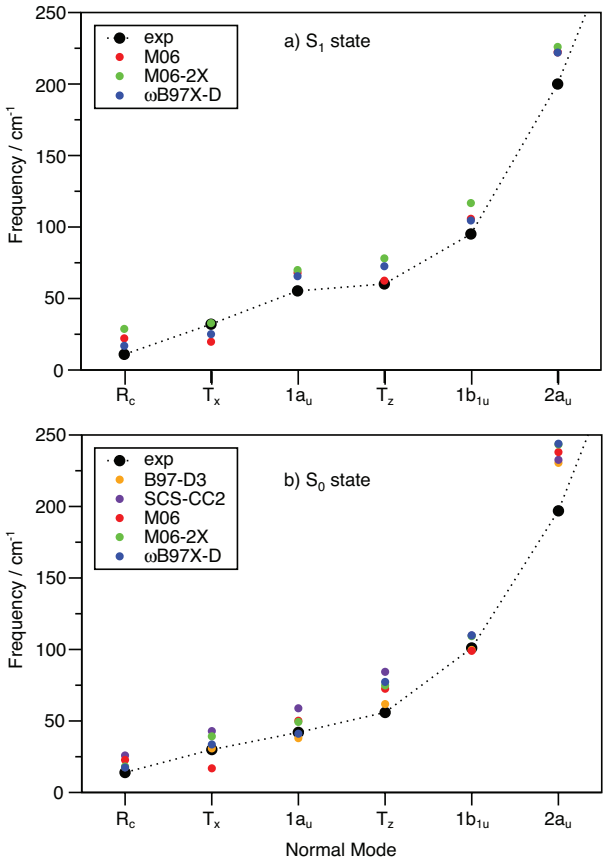

Figure 11: Calculated (color) and experimental (black) intermolecular vibrational frequencies of the experimentally observed vibrations of perylene·tetrachloroethene in the S_0 (bottom) and S_1 (top) states.

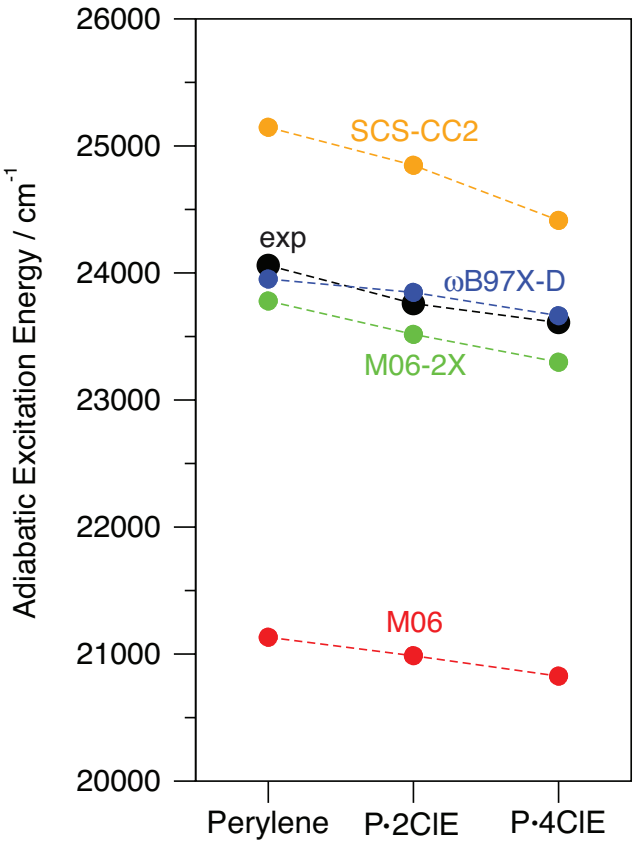

Figure 12: Comparison of experimental (in black) and calculated (color) $S_0 \rightarrow S_1$ adiabatic excitation energies of perylene, perylene·1,2-dichloroethene (from ref. 7 and perylene·tetrachloroethene (this work).

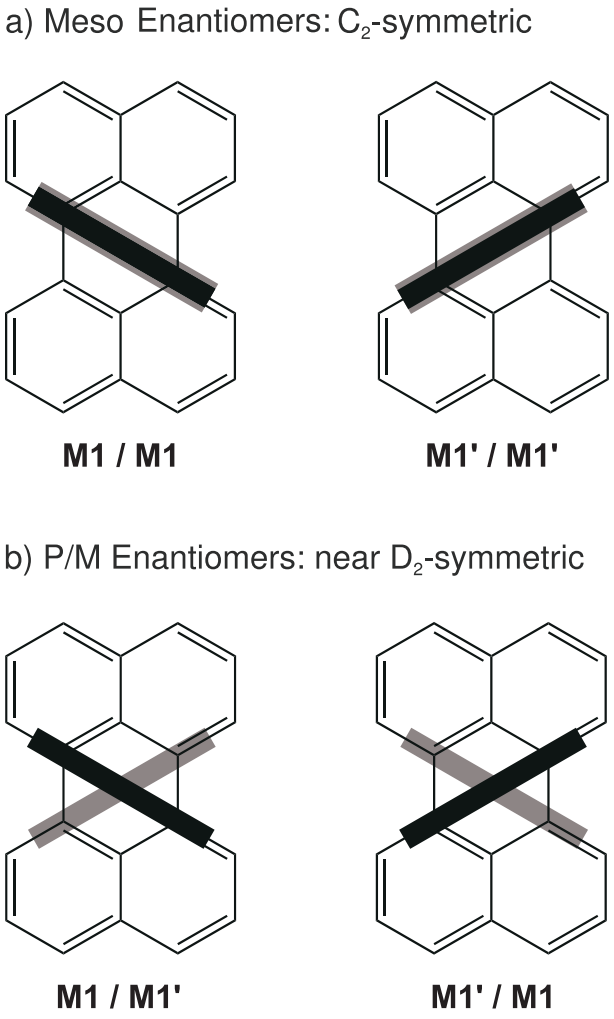

Figure 13: Schematic representations of the two structure types and respective enantiomers of perylene·(tetrachloroethene)$_2$. (a) *meso* forms, (b) plus/minus (P/M) enantiomers.

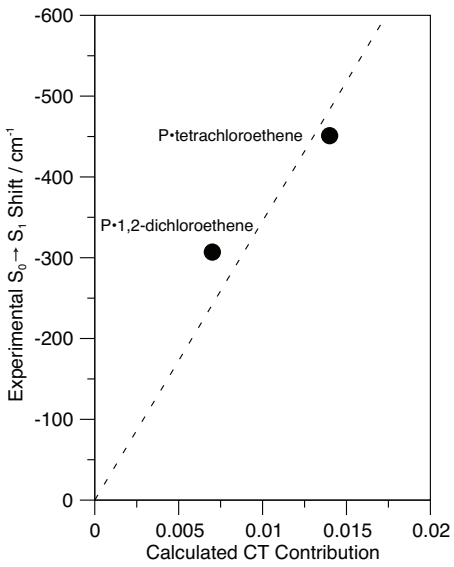

Figure 14: Plot of the experimental $S_0 \rightarrow S_1$ spectral shifts of perylene·-1,2-dichloroethene and perylene·tetrachlorethene vs. the calculated charge-transfer contribution, as computed by the TheoDORE method,[31] using the SCS-CC2/TZVP transition density matrices.

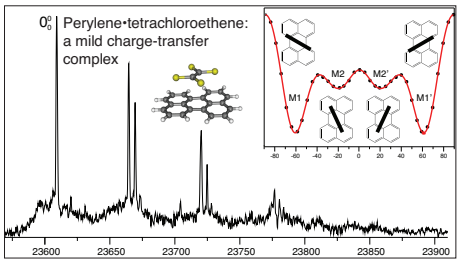

Figure 15: TOC Graphic